Available online at www.sciencedirect.com
SCIENCE DIRECT
Scripta Materialia 55 (2006) 343–346
Scripta MATERIALIA
www.actamat-journals.com

Hydraulically pumped cone fracture in bilayers with brittle coatings

Herzl Chai[a] and Brian R. Lawn[b,*]

[a] *Department of Solid Mechanics, Materials and Systems, Tel Aviv University, Tel Aviv, Israel*
[b] *Materials Science and Engineering Laboratory, National Institute of Standards and Technology, Gaithersburg, MD 20899-8500, USA*

Received 9 February 2006; revised 11 April 2006; accepted 26 April 2006
Available online 22 May 2006

An earlier finite element modeling analysis of inner cone cracks in monolithic brittle solids subject to cyclic indentation in liquids is extended to include the case of a brittle layer bonded to a compliant substrate, using a model glass/polycarbonate bilayer system as an illustrative case study. Provision is made for incorporation of plate flexure stresses, along with hydraulic pumping stresses, into the Hertzian contact field. Tensile flexure stresses ultimately accelerate inner cone cracks through the lower halves of the glass plates to unstable failure. The analysis accounts for the experimentally observed trends in the inner cone crack evolution in cyclic contact fatigue.

Keywords: Bilayers; Brittle coatings; Cyclic contact; Hydraulic pumping; Inner cone cracks

When a thick brittle solid monolith is subjected to spherical indentation in single-cycle loading in air, a shallow cone crack initiates immediately outside the expanding contact circle [1–3]. In cyclic contact in water, a second kind of cone crack forms well within the maximum contact circle [4,5]. These two cone crack types, designated outer (O) and inner (I), are depicted schematically in Figure 1. The inner cone crack is steeper than its outer counterpart, and propagates deeper in extended cycling. Inner cone cracks have also been observed in bilayer structures with brittle coatings used to simulate biomechanical prostheses – particularly dental crowns in occlusal function [5]. In persistent cycling loading in water, these inner cone cracks may propagate entirely through the coating layer, with acceleration in the lower half of the plate, resulting in through-thickness failure.

Here, we seek to quantify this behavior by extending a preceding finite element model (FEM) for cone crack evolution in monolithic brittle solids subject to cyclic loading with a hard sphere in water [6]. In that preceding paper, cone cracks initiating outside (O) and inside (I) the contact circle were analyzed in stepwise manner through the oscillating Hertzian field, at each step determining the next incremental crack path and associated stress-intensity factor. A crack velocity relation was used to determine the size of each crack kink increment. Due allowance was made for hydraulic pressure at the inner cone crack walls, from ingress and egress of liquid from the crack interface [7,8]. Three evolutionary stages were identified: a surface flaw extends by slow crack growth into a shallow cone; hydraulic pumping becomes effective, driving the cone crack through the subsurface compression zone under the indenter; the hydraulic forces die out and the crack enters the contact far field.

The case of bilayers differs from that of the monolith primarily by superposition of plate flexure stresses in the coating layer – compression in the top part of the coating and tension in the bottom part. We focus on the role of this flexural component in determining the crack evolution during cycling, especially crack acceleration in the later stages of crack growth leading to failure. The bilayer system under specific consideration here is that of a glass plate bonded to a compliant polymeric substrate, for which contact fatigue data are available [9]. Our results will confirm that inner cone cracks can be a potent failure mode in brittle layer systems subject to cyclic concentrated loading in liquid environments.

Figure 2 shows the crack profile for a 1 mm thick soda-lime glass plate bonded to a polycarbonate base, for cycling at 1 Hz with a 1.58 mm WC sphere at maximum load $P_m = 120$ N in water. The image is a post-test section through an indentation center, polished (1 μm diamond paste) and lightly etched (10% HF for 30 s) to enhance the crack profiles (“section-and-etch” technique [10]). The section shows several shallow cracks

* Corresponding author. E-mail: brian.lawn@nist.gov

1359-6462/$ - see front matter © 2006 Acta Materialia Inc. Published by Elsevier Ltd. All rights reserved.
doi:10.1016/j.scriptamat.2006.04.035

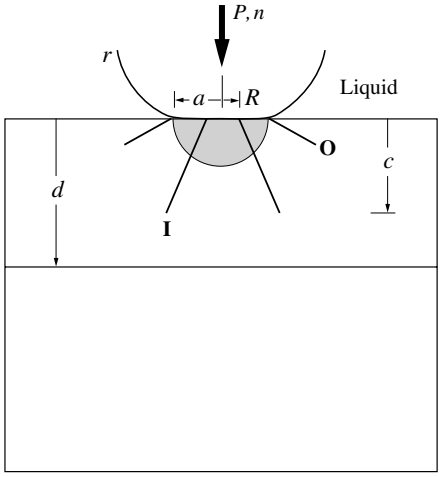

Figure 1. Schematic of cone crack system in bilayer consisting of brittle plate of thickness d on compliant support. Spherical indenter, sphere radius r, contact radius a, load P and cycles n. Label O designates outer cones, I denotes inner cones. Inner cone crack located distance R from contact axis shown at depth c. Shaded area indicates compression zone below contact. Contact occurs in liquid.

near the surface, with one dominant inner cone leading to through-thickness plate failure.

Examination of several profiles of the kind shown in Figure 2 revealed a somewhat shallower crack path in the glass bilayers relative to glass monoliths, an average ≈30° instead of ≈50° [5,6]. Closer inspection also revealed the location R of the critical I cracks to be a little larger in the bilayers, by about 20%.

Full evolution of cone cracking is more easily monitored in glass-based systems by direct in situ viewing with a video camera during testing [11]. Crack depth data c as a function of number of cycles n using a WC sphere with radius $r = 1.58$ mm at maximum load $P_m = 120$ N are shown in Figure 3 for (a) monolithic glass and (b) 1 mm glass on polycarbonate. These data, taken from previous experimental studies [9,12,13], indicate essential differences between monolith and bilayer responses. The outer cone cracks (O) are smaller in the bilayer specimens over the entire cycling range, consistent with the superposition of compressive flexural stresses onto the Hertzian field in the top portion of the plate. The inner cone cracks (I), dominant after $n \approx 10^3$ cycles, ultimately become more unstable in the bilayers, accelerating toward the glass/polycarbonate interface with consequent plate failure after extensive cycling (arrows).

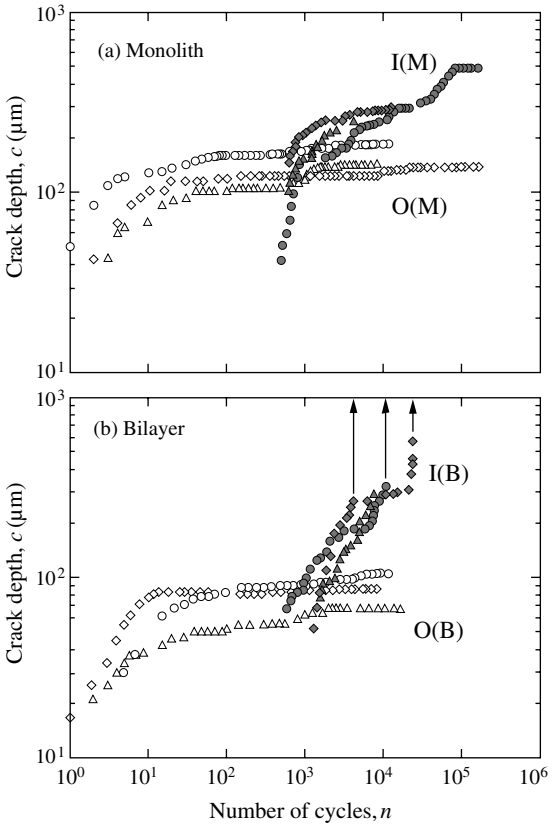

Figure 3. Experimental data showing evolution of outer (O) and inner (I) cone crack depth c with number of cycles n for (a) monolith soda-lime glass and (b) glass plate of thickness $d = 1$ mm bonded to polycarbonate base. Each symbol represents a different test. Arrows in (b) denotes failure instabilities. Indentation with WC sphere $r = 1.58$ mm, maximum load $P_m = 120$ N, frequency $f = 1$ Hz, in water. Data from previous papers [9,12,13].

The procedure in the FEM code, outlined in detail in the preceding paper on monoliths [6], is to introduce a starting surface flaw of depth 1 μm at a prescribed location R and to allow this flaw to extend stepwise into a flared cone beneath the material surface. At each step, stress-intensity factors are evaluated using the Irwin near-field relations for crack-wall displacements. The preferred incremental path kink is determined as that for which K_I is maximum and $K_{II} = 0$. A crack velocity relation for the specific material/environment system is used to determine the extension increment during each cycle. Provision is made for ingress of liquid into inner cone cracks during the expanding contact and for the

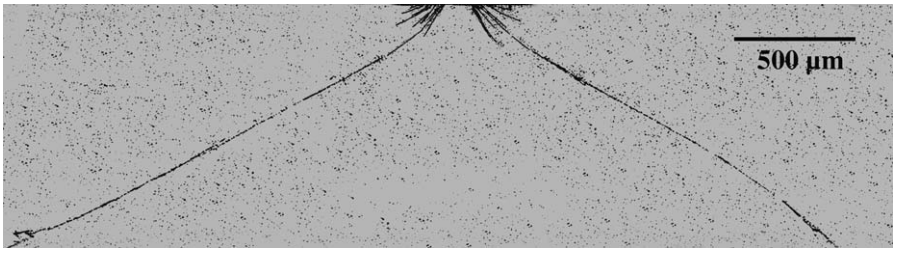

Figure 2. Section views through cracks formed in a glass plate of thickness $d = 1$ mm bonded to polycarbonate base, subject to indentation with WC sphere of radius $r = 1.58$ mm, maximum load $P_m = 120$ N, $n = 25 \times 10^3$ cycles at frequency $f = 1$ Hz, in water. Steep inner cone crack traces are evident. (Only glass layer shown. Image digitally enhanced to emphasize crack profile.)

superposition of crack-wall stresses from squeezing of the entrapped liquid after contact engulfment, assuming the fluid to be incompressible [8].

In the present study, the system to be investigated is that of a soda-lime glass plate of thickness $d = 1$ mm bonded to a thick polycarbonate base, subject to cyclic contact in water with a WC sphere with $r = 1.58$ mm at $P_m = 120$ N. Input elastic moduli and Poisson's ratios are, respectively: coating, 70 GPa and 0.22; base, 2.35 GPa and 0.35; indenter, 614 GPa and 0.22. For comparison purposes, starting crack locations are taken to be the same as for glass monoliths [6], i.e. $R = 65$ μm ($=0.50\,a_m$) for the inner cone and $R = 150$ μm ($=1.15\,a_m$) for the outer cone (a_m = maximum contact radius).

Figure 4 compares computed outer (O) and inner (I) crack profiles for glass/polycarbonate bilayers (B), with those for glass monoliths (M) included for comparison. Both O and I cones follow significantly more shallow paths than in the monoliths, consistent with experimental observation.

Figure 5 plots stress-intensity factors K pertinent to the crack paths in Figure 4 as a function of cone depth c. Comparing the $K(c)$ curves for bilayers (B) with 1 mm thick glass on polycarbonate with those for glass monoliths (M) reveals certain trends. Starting with outer cone cracks (O), the B curve shows an initial depression relative to the M curve, consistent with the superposition of compressive flexural stresses onto the Hertzian field in the top half of the plate. At a depth $c \approx 200$ μm the B curve crosses the M curve and rises rapidly, indicative of dominant tensile flexural stresses in the lower half of the plate. An analogous trend is apparent with inner cone cracks (I), i.e. an initial depression of the B versus M curve and subsequent rapid rise beyond a crossover point at $c \approx 400$ μm. The I curves initially fall well below the O curves, indicating a more sluggish initiation stage, but rise above the O curves in the later stages of growth, confirming an inner cone crack mode of failure under these cyclic loading conditions.

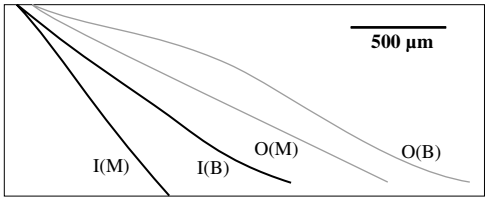

Figure 4. Calculated crack profiles for outer (O) and inner (I) cone cracks in monolith glass (M) and bilayer glass/polycarbonate (B), for $P_m = 120$ N and $r = 1.58$ mm. Starting locations are $R = 150$ μm for the outer cone and $R = 65$ μm for the inner cone.

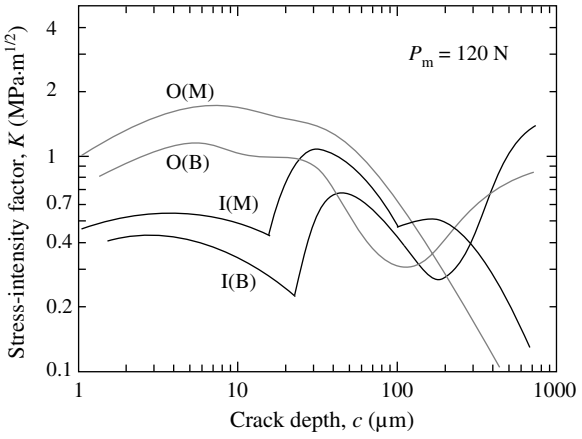

Figure 5. Mode-I stress-intensity factor K as a function of crack depth c for outer (O) and inner (I) cone cracks in monolith glass (M) and bilayer glass/polycarbonate (B), for experimental conditions represented in Figure 3 and for locations represented in Figure 4.

The existence of the pronounced humps in Figure 5, corresponding to the superposition of hydraulic pumping forces onto the Hertzian field, warrants special comment. These forces are effective between $c \approx 10$–20 μm and $c \approx 100$–200 μm, i.e. in the depth range of the compression zone beneath the Hertzian contact [6]. It is these humps that largely drive the crack through the compression zone to the Hertzian far field.

In this paper we have extended an earlier FEM analysis of inner cone cracks in monolithic brittle solids subject to cyclic indentation in liquids [6] to the case of a brittle layer bonded to a compliant substrate, specifically glass plates on polycarbonate substrates tested in water with a specified spherical indenter at a specified load condition. The bilayer is distinguished by the superposition of plate flexure stresses onto a Hertzian contact field, in which tension in the lower half of the plate induces a state of instability in the crack evolution, leading to through-thickness failure. Provision is preserved for hydraulic pumping at the inner cone crack walls, enabling initial penetration through the immediate contact zone into the far-field region. The computations account for all the basic data trends, most notably an initial inhibition of crack growth in the upper half of the plate and, more significantly, subsequent instability in the lower half of the plate.

Such FEM computations are complex and time consuming, especially in the regions where hydraulic pumping occurs, and are sensitive to assumptions in the crack configurations [6]. For instance, the $K(c)$ minima in the I(B) curve in Figure 5 lie close to the threshold for water-assisted crack growth in soda-lime glass [14,15], suggesting that the I cracks would have difficulty initiating and propagating through the near field. The tendency for the dominant inner cone crack has been discussed earlier as to lie a little more distant from the contact center in the bilayers. This feature has been neglected in the FEM analyses embodied in Figures 4 and 5. Repeating the calculation with relocation of the inner cone trace from $R = 65$ μm to $R = 80$ μm shifts the $K(c)$ curve upward in the region of the minima by ≈30%, i.e. above the threshold for slow crack growth. Interaction with adjacent cracks in the near-surface region (e.g. Fig. 2) may further influence the initiation stages of growth. It is because of this sensitivity to input assumptions that we have not attempted to compute absolute $c(n)$ curves for comparison with the data in Figure 5.

Notwithstanding these variants, the calculations confirm the viability of hydraulic pumping as a potent driving force in the evolution of inner cone cracks in brittle layer structures.

This work was supported by a grant from the US National Institute of Dental and Craniofacial Research (PO1 DE10976).

[1] F.C. Frank, B.R. Lawn, Proc. R. Soc. London, A 299 (1967) 291.
[2] T.R. Wilshaw, J. Phys. D: Appl. Phys. 4 (1971) 1567.
[3] B.R. Lawn, J. Am. Ceram. Soc. 81 (1998) 1977.
[4] D.K. Kim, Y.-G. Jung, I.M. Peterson, B.R. Lawn, Acta Mater. 47 (1999) 4711.
[5] Y. Zhang, J.-K. Kwang, B.R. Lawn, J. Biomed. Mater. Res. 73B (2005) 186.
[6] H. Chai, B.R. Lawn, Acta Mater. 53 (2005) 4237.
[7] S. Way, J. Appl. Mech. 2 (1935) 49.
[8] A.F. Bower, J. Tribol. 110 (1988) 704.
[9] S. Bhowmick, Y. Zhang, B.R. Lawn, J. Mater. Res. 20 (2005) 2792.
[10] A.G. Mikosza, B.R. Lawn, J. Appl. Phys. 42 (1971) 5540.
[11] H. Chai, B.R. Lawn, S. Wuttiphan, J. Mater. Res. 14 (1999) 3805.
[12] Y. Zhang, B.R. Lawn, Key. Eng. Mater. 284–286 (2005) 697.
[13] Y. Zhang, S. Bhowmick, B.R. Lawn, J. Mater. Res. 20 (2005) 2021.
[14] S.M. Wiederhorn, L.H. Bolz, J. Am. Ceram. Soc. 53 (1970) 543.
[15] K.-T. Wan, S. Lathabai, B.R. Lawn, J. Eur. Ceram. Soc. 6 (1990) 259.